ACS APPLIED MATERIALS & INTERFACES

ACS AUTHORCHOICE

www.acsami.org

Research Article

On the Origin of the OER Activity of Ultrathin Manganese Oxide Films

Paul Plate, Christian Höhn, Ulrike Bloeck, Peter Bogdanoff, Sebastian Fiechter, Fatwa F. Abdi, Roel van de Krol,* and Aafke C. Bronneberg

Cite This: *ACS Appl. Mater. Interfaces* 2021, 13, 2428–2436

Read Online

ACCESS | Metrics & More | Article Recommendations | Supporting Information

ABSTRACT: There is an urgent need for cheap, stable, and abundant catalyst materials for photoelectrochemical water splitting. Manganese oxide is an interesting candidate as an oxygen evolution reaction (OER) catalyst, but the minimum thickness above which MnO_x thin films become OER-active has not yet been established. In this work, ultrathin (<10 nm) manganese oxide films are grown on silicon by atomic layer deposition to study the origin of OER activity under alkaline conditions. We found that MnO_x films thinner than 1.5 nm are not OER-active. X-ray photoelectron spectroscopy shows that this is due to electrostatic catalyst−support interactions that prevent the electrochemical oxidation of the manganese ions close to the interface with the support, while in thicker films, Mn^{III} and Mn^{IV} oxide layers appear as OER-active catalysts after oxidation and electrochemical treatment. From our investigations, it can be concluded that one $Mn^{III,IV}$−O monolayer is sufficient to establish oxygen evolution under alkaline conditions. The results of this study provide important new design criteria for ultrathin manganese oxide oxygen evolution catalysts.

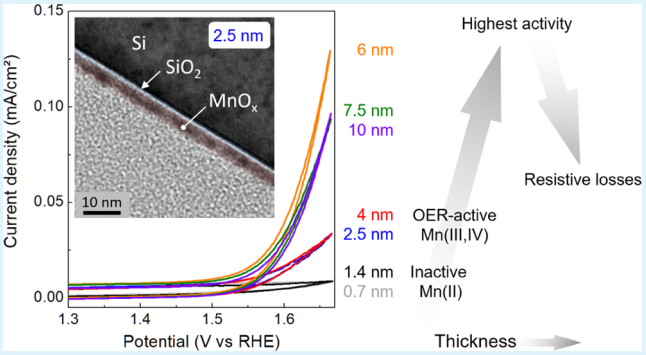

KEYWORDS: *electrocatalysis, oxygen evolution, ALD, MnO_x, X-ray photoelectron spectroscopy, electrochemistry*

INTRODUCTION

To combat the adverse effects of greenhouse gas emissions, there is a clear and urgent need for new sustainable ways to generate and store energy in a scalable manner. A promising route for this is to generate hydrogen by solar-powered water splitting. This offers a pathway to simultaneously harvest sunlight and store it in the form of chemical bonds. A convenient and technologically mature solution to generate such a "solar fuel" is to couple a photovoltaic cell to an electrolyzer, usually with a dc−dc converter. Alternatively, a photoelectrochemical approach based on chemically stable semiconductor photoelectrodes immersed directly in water is being pursued; an important advantage of the latter approach is that the kinetics of the electrochemical reactions are enhanced by solar heating of the device.[1] Both approaches typically require electrocatalysts for the hydrogen and oxygen evolution reactions. These catalysts should be cheap and abundant, have modest overpotentials for the reactions of interest, and show excellent chemical stability.[2−5]

A potentially interesting catalyst for the oxygen evolution reaction (OER) is manganese oxide (MnO_x). Its activity is well known from photosystem II, where manganese is present in a biochemical cluster.[6,7] Much effort has been made to synthesize MnO_x as an artificial OER catalyst. First reports on this material date back to 1977, when the first electrochemical depositions of this material were reported.[8] Since then, many follow-up studies on this oxide have been carried out to understand what defines the catalytic activity of MnO_x.[9−14] For an overview of the recent state of the art in MnO_x OER catalysts and the current state of understanding, the reader is referred to two recent reviews.[15,16] One important factor that determines the catalytic activity is the chemical structure of manganese-based catalysts. One generally needs to "activate" MnO_x and other transition-metal oxide OER catalysts by several anodic potential sweeps. Such activation pretreatments have been shown to lead to structural changes at the surface,[17] which seem to be necessary to create the optimal local atomic structure around the catalytically active Mn sites. Specifically, using in situ X-ray absorption spectroscopy, Gorlin et al.[18] showed that the average oxidation state of Mn increases to 3.6 during activation and that this is accompanied by the formation of a birnessite-type layer structure. This structural transformation is believed to be an important step in the

Received: September 4, 2020
Accepted: December 30, 2020
Published: January 11, 2021

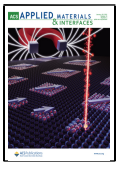

https://dx.doi.org/10.1021/acsami.0c15977
ACS Appl. Mater. Interfaces 2021, 13, 2428–2436

formation of active MnO_x, since K- and Ca-doped manganese oxides with the same birnessite structure are among the best-performing manganese oxide OER catalysts.[9,19−21] However, the key parameter seems to be the manganese oxidation state.[4,20,22−24] Ramírez et al.[4,12] have shown that the Mn oxidation state has a major influence on performance in terms of onset potential and current density. The results suggest that a mixture of +III and +IV oxidation states is needed to obtain an active OER catalyst.[18,24] When integrating MnO_x as a catalyst in a photoelectrochemical device, three main issues have to be overcome: (1) the parasitic optical absorption of the manganese film, (2) resistive losses due to poor electronic conductivity of the film, and (3) electrochemical stability.

The latter (which was not a central part of our investigation) has been studied by different authors[4,5,16,25−27] under alkaline and acidic conditions. Even at a high current density of 10 mA/cm^2, electrodes consisting of α-Mn_2O_3 nanoparticles—the surfaces of which were covered by an amorphous Mn^{IV}-containing oxide of about 0.7 nm thickness—were stable at potentials ≤1.7 V vs RHE under alkaline conditions.[5] Comparing the stabilities of different manganese oxides, it could be demonstrated that the Mn^{III} oxide in the presence of an ultrathin thin amorphous Mn^{IV} oxide film on top turned out to be more stable than a pure Mn^{IV} oxide film of γ-MnO_2.[4] However, Li et al. demonstrated that γ-MnO_2 deposited on FTO and on carbon support, respectively, exhibited an electrochemical stability for 6000 h under OER conditions in a 1.0 M H_2SO_4 electrolyte in a potential window of 1.6−1.75 V vs RHE.[25] The authors explain this extraordinary stability by a balance between dissolution and redeposition of Mn ions in the chosen potential window. This hypothesis was confirmed by Rabe et al.[26] They investigated MnO_x phase formation under alkaline conditions starting from metallic Mn. With increasing potential from −0.5 to 1.75 V vs RHE in an alkaline 0.1 M NaOH electrolyte, they noted four oxidation waves in the first CV sweep, which were explained by a progressive oxidation of the metallic manganese in a first step to $Mn(OH)_2$. Then, the oxidation of Mn_3O_4, in two further steps, to Mn_2O_3 and MnO_2 was observed as expected from the Pourbaix diagram.[25] A reversible reduction−oxidation reaction was found afterward in the range of Mn_2O_3 and MnO_2 formation in the second sweep. Using a scanning flow cell connected to an inductively coupled plasma mass spectrometer (ICP-MS), they noted the redeposition under formation of a strongly disordered β-MnO_2 under OER conditions.

Stability as a function of pH was also investigated by Melder et al.[16] studying the electrochemical stability of birnessite in a pH range of 5−9. Best results were found using a 0.5 M phosphate buffer solution at pH 7 at a current density of 1 mA/cm^2. Indeed, the treatment of MnO_x electrodes in a phosphate buffer solution contributes to an increase in electrochemical stability presumably due to the formation of stable manganese phosphate complexes at the electrode/electrolyte interface.[4]

Besides questions of the electrochemical stability of the different MnO_x phases, the oxidation state of the metals in manganese oxides at the electrode/electrolyte interface plays a crucial role. Using X-ray absorption spectroscopy, Shaker et al. studied MnO_x phase formation from an ionic liquid under acidic, neutral, and alkaline conditions. In all cases, no single-phase films were obtained. The most catalytically OER-active electrode consisted of Mn_2O_3 and a birnessite-type phase with a minimal amount of Mn_3O_4. It was hypothesized that enhanced catalytic OER activity could be associated with structural disorder and distortions (in the coordination polyhedral) of the different oxides, leading to an interaction of different MnO_x phases in the catalytic process.[28]

The influence of parasitic optical absorption of the manganese film and resistive losses can be tackled using ultrathin films, as we will show in this paper. A viable method to deposit such films in a controlled manner is atomic layer deposition (ALD). ALD has the following two key advantages over other deposition techniques, such as physical vapor deposition[29] or electrodeposition:[4,5] atomic-level control over the thickness of the film and the ability to conformally coat high-aspect-ratio surface structures. Especially, the possibility to coat complex topographies makes ALD an ideal deposition technique for electrodes in (photo)electrochemical devices, since these are often designed to have large specific surface areas and high aspect ratios.

ALD processes of MnO_x have already been reported using, e.g., $Mn(EtCp)_2$ or $Mn(tBu\text{-}MeAMD)_2$ as a manganese precursor and water as an oxidant.[30−33] The resulting MnO_x films were found to be stable and active toward the OER, and a similar relationship between the oxidation state and the activity of these thin films has been found as for non-ALD films.[22,31,32] However, the majority of these studies focused on films thicker than 25 nm, even though further thickness minimization may lower the parasitic absorption and avoid current losses due to the ohmic resistance. Strandwitz et al. executed a first study of films thinner than 25 nm, which were used to protect n-type silicon photoanodes. They found that films thicker than 4 nm suffered from resistive losses, while thinner films provided insufficient protection of the silicon.[32] As a consequence, the OER activity of ultrathin films (<4 nm) has not yet been explored. It is, therefore, unclear how much further the film thickness can be reduced before the OER activity drops too much.

In this study, we address the origin of the OER activity of ultrathin MnO_x films grown by ALD. We focus our efforts on alkaline solutions since the OER generally proceeds at higher rates at high pH values.[16] The thin-film region (0.7−10 nm) is spectroscopically and electrochemically characterized and evaluated with respect to the OER activity. Prior to oxygen evolution, OER-active MnO_x films undergo an oxidation process, which alters the dominant oxidation state from Mn(II/III) to Mn(IV). We will show that this oxidation can only occur when there is a certain minimum amount of oxidizable Mn ions in the film and that this leads to a minimum MnO_x film thickness for OER-active films.

EXPERIMENTAL DETAILS

Manganese oxide thin films were deposited on silicon substrates (Si Mat) using a home-built, hot-wall atomic layer deposition reactor.[34] N-type silicon ([100], phosphorus-doped, ρ = 1−10 Ω/cm^2) and p^{++}-type silicon ([100], boron-doped, ρ = 3−10 Ω/cm^2) were used for optical analysis and electrochemical characterization, respectively. Prior to deposition, the substrates were cleaned by ultrasonication in Millipore water and dried in a nitrogen flow (99.999%).

The ALD reactor was constantly pumped by a turbo molecular pump backed up by a roughing pump, resulting in a base pressure in the lower 10^{-7} mbar range. Bisethylcyclopentedienyl manganese ($(EtCp_2)Mn$, Strem Chemicals, 98.5%), kept at 85 °C, and water (Millipore, 18.2 MΩ) were used as Mn and oxygen precursors, respectively. The reactor wall was heated to 125 °C, while the substrate temperature was kept at 150 °C. The Mn precursor and water were each dosed for 1.5 s. After each precursor exposure, a

https://dx.doi.org/10.1021/acsami.0c15977
ACS Appl. Mater. Interfaces 2021, 13, 2428−2436

pump/purge/pump step was carried out, consisting of 30 s pumping/0.1 s Ar dose/30 s pumping. This leads to a growth per cycle (GPC) of 1.3 Å/cycle. The saturation curves, the temperature window, and proof of linear growth are shown in Figure S1a–d. Some of the films were chemically oxidized by exposure to an oxygen plasma. This was done immediately after the growth of the films, using the radio frequency plasma generator (MANTIS) that is part of the ALD reactor. For plasma exposure, an oxygen partial pressure of 4×10^{-5} mbar (gas purity, 99.999%) and a plasma power of 200 W were used.

The ALD reactor is connected via a UHV buffer chamber (2×10^{-10} mbar) to a UHV chamber equipped for X-ray and ultraviolet photoelectron spectroscopy (XPS and UPS). This allows for in-line transfers in between the ALD (half-)cycles, thereby preventing surface contamination due to air exposure. XPS measurements were carried out using an Al Kα X-ray source (1486.74 eV) and a hemispherical XPS analyzer (SPECS Phoibos 100) equipped with a SPECS FOCUS 500 monochromator. UPS measurements were carried out using a helium discharge lamp emitting He Iα (21.22 eV) radiation. Survey and fine spectra were collected at a normal angle from the surface, except when stated otherwise. The pass energy was set to 30 and 10 eV for the survey and fine spectra, respectively, with step sizes of 0.5 and 0.05 eV. Voigt profiles and Shirley background subtraction were used to fit the photoemission lines in the fine spectra. All spectra were calibrated with respect to the C 1s peak at 284.5 eV.

The film thickness was determined ex situ using spectroscopic ellipsometry (J.A. Woollam Co., M-2000D, 193–1000 nm). The dielectric function of the MnO_x films was modeled with a Tauc–Lorentz dispersion equation.[35] Electrochemical characterization was performed in a three-electrode configuration. A Ag/AgCl/sat. KCl electrode (Radiometer Analytical XR 300) and a platinum mesh were used as reference and counter electrodes, respectively. The ohmic contact was made by scribing a Ga–In eutectic (Alfa Aesar, 99.99%) on the unpolished backside of the p^{++}-Si substrate onto which a gold spring was pressed. An aqueous solution of 0.1 M KOH (Sigma-Aldrich) was used as the electrolyte (pH 13). The area exposed to the electrolyte was 0.2 cm^2 for all measurements. Electrochemical measurements were made using a VersaSTAT 3 potentiostat from Princeton Applied Research. All electrochemical potentials were converted to the reversible hydrogen potential (RHE) scale. Cyclic voltammetry measurements were performed at a scan rate of 2 mV/s, unless stated otherwise. To perform the iR correction, electrochemical impedance spectroscopy at a potential that corresponds to the open-circuit potential was executed (1 MHz to 0.1 Hz, 10 mV modulation amplitude). The high-frequency intercept was used to determine the cell resistance R_{cell}, which varied between 100 and 200 Ω. This value was used together with eq 1 to correct the applied potential, $U_{applied}$.

$$U_{real} = U_{applied} - IR_{cell} \quad (1)$$

Here, U_{real} and I are the corrected potential and the measured current, respectively. The potential correction was typically less than 30 mV and never more than 90 mV.

RESULTS AND DISCUSSION

Film Structure. Figure 1 shows the TEM images of as-deposited MnO_x films with thicknesses of 2.5, 5.5, 10, and 18 nm. The MnO_x film is highlighted in brown; the native silicon oxide is highlighted in light blue. The MnO_x films appear to be predominantly amorphous, interspersed with nanometer-sized crystallites (highlighted by oval shapes). These crystallites are formed after the growth of at least 0.5 nm of amorphous MnO_x. Beyond this initial amorphous stage, the films show varying degrees of crystallinity. With increasing film thickness, the overall crystallinity and the crystallite sizes increase. The individual crystallites have random crystallographic orientations. Using the distance between the silicon atoms of the silicon substrate as internal reference (Si–Si distance, 0.234 nm[36]), an average lattice plane distance of 0.27 ± 0.07 nm was found, which is an excellent fit to the (111) lattice plane distance of 0.271 nm in α-Mn_2O_3. The surface of the films is very smooth; AFM images (Figure S3) reveal surface roughnesses of 0.3, 0.1, 0.6, and 0.7 nm for the 2.5, 5.5, 10, and 18 nm films, respectively. It should be noted, however, that with an AFM tip radius of ∼10 nm, the nanometer-sized irregularities that can be observed in the TEM images in Figure 1 will not be apparent in the AFM data. The surface roughness for the 10 nm film seems slightly larger than for the other films, the reason for which is not clear. Nonetheless, these ALD-grown films on silicon wafers are likely to be among the flattest MnO_x films reported in the literature thus far, and are considered to be without significant structural topography for the purposes of this study.

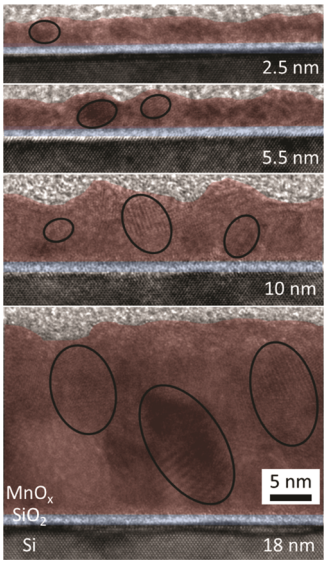

Figure 1. TEM images of as-deposited MnO_x films on Si, with film thicknesses of 2.5, 5.5, 10, and 18 nm. The MnO_x films (highlighted in brown) are predominantly amorphous, interspersed with nanometer-sized crystallites (highlighted by oval shapes). The native oxide is highlighted in light blue. The coloring was done by hand; the original TEM image is shown in Figure S2 in the Supporting Information.

Surface Composition. Figure 2a–c shows the Mn 2p fine spectra of MnO_x films (a) after an in-line transfer, (b) after air exposure, and (c) after electrochemistry. Each spectrum consists of Mn $2p_{3/2}$ and $2p_{1/2}$ peaks with a spin–orbit splitting (S.O.S) of 11.7 eV. Satellite features of the $2p_{3/2}$ and $2p_{1/2}$ peaks can be found in the binding energy range of 646–649 and 659–670 eV, respectively. These S.O.S. values identify our manganese compound as an oxide.[37] However, it does not provide information on the Mn oxidation state, which is a key parameter governing the catalytic activity.[4] Two approaches are commonly used to determine the Mn oxidation state in MnO_x. One approach, reported by Gorlin et al.,[23] uses the distance between the Mn $2p_{1/2}$ peak (∼653 eV) and the corresponding satellite feature (i.e., 670–659 eV). They found a correlation between this distance and the main oxidation state of manganese for several manganese oxides. The second approach, reported by Biesinger et al., is to fit the Mn $2p_{3/2}$ feature with a series of peaks that reflect the extensive multiplet splitting that is observed for most of the oxidation states of manganese.[37] The fitting parameters that they reported were used as the starting point for identifying the Mn oxidation states in our ALD films.

https://dx.doi.org/10.1021/acsami.0c15977
ACS Appl. Mater. Interfaces 2021, 13, 2428–2436

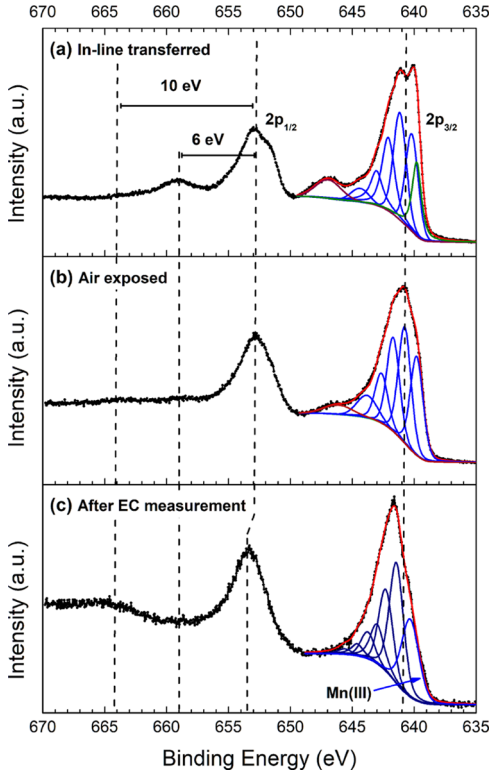

Figure 2. XPS spectra of the Mn 2p region (a) after deposition using an in-line transfer, (b) after air exposure, and (c) after electrochemistry. Details about peak parameters can be found in the Supporting Information.

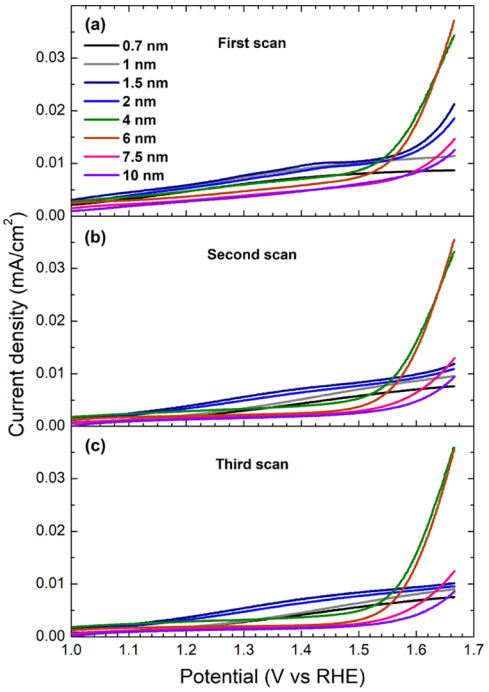

Figure 3. First three voltammograms (a–c) of MnO_x catalyst films of different thicknesses deposited on p^{++}-Si. All data are iR-corrected.

For the as-deposited, in-line transferred film, the distance between the satellite peak and the $2p_{1/2}$ peak equals 6 eV (Figure 2a). According to Gorlin et al., a separation of 6 eV is typical for MnO compounds in which Mn has an average oxidation state of +II.[23] This is consistent with the analysis using Biesinger's approach, for which the best deconvolution was achieved using a Mn(II)O multiplet pattern.[36] After the deconvolution, an additional peak remains at 639.5 eV (green curve in Figure 2a). This peak is assigned to manganese in a metallic state.[4]

When the film is exposed to air, the corresponding spectrum changes. This change is visible by a decrease in intensity of the satellite feature at 659 eV and the appearance of another (very weak) satellite feature at 663 eV (Figure 2b). A distance of 10 eV between this new satellite feature (663 eV) and the manganese $2p_{1/2}$ peak (653 eV) would suggest an average oxidation state of +III.[23] However, the satellite features at 663 and 659 eV are too weak for a definite assignment. Instead, multiplet peak patterns for Mn_2O_3 and MnO were used to fit the spectrum. Only the MnO pattern leads to complete deconvolution. Moreover, the metallic species is no longer observed. From this, we conclude that only manganese oxide in the oxidation state +II is present after air exposure.

After three linear sweep voltammograms between 1.0 and 1.7 V vs RHE (data shown in Figure 3; see discussion below), the film oxidizes further. As shown in Figure 2c, the satellite feature at 663 eV is now clearly visible, while the satellite feature at 659 eV has almost completely disappeared. The best deconvolution was achieved using MnO_2 multiplet pattern with an added peak at a binding energy of 640.5 eV. Biesinger et al.[37] reported a similar peak pattern and attributed the additional peak to manganese in the oxidation state of +III. Based on this observation, we conclude that the average manganese oxidation state after electrochemistry is between three and four. This has also been observed by Gorlin et al.[18]

We also measured the O 1s spectra of the films during growth by transferring the sample from the ALD chamber to the XPS chamber under UHV conditions after successive ALD cycles. The results are shown in Figure S4a. As expected, the O 1s signal for the Si/SiO_2 substrate at ~530.9 eV decreases, while the O 1s signal for MnO_x at 528.6 eV increases with increasing film thickness. Based on the ALD growth mechanism, illustrated in Figure S4b, the MnO_x films are expected to be hydroxylated. Unfortunately, the O 1s signal from the SiO_2 layer completely masks the O 1s signal from the OH groups, which also lies at 530.9 eV (as shown by the clear OH signal for thicker MnO_x films; see Figure S4c). This raises the question whether the thinnest films are also hydroxylated. We do not have direct evidence for this, but if the films were not hydroxylated, we would expect a nucleation delay in the initial stages of ALD growth (since the ALD precursor reacts with the −OH groups at the surface). As shown in Figure S1d, no nucleation delay is observed, which makes it likely that the MnO_x surface is −OH-terminated during all stages of growth.

Effect of MnO_x Film Thickness on OER Activity. To determine the thickness at which MnO_x becomes catalytically active, p^{++}-Si/MnO_x anodes with different MnO_x thicknesses (0.7–10 nm) were prepared and CV scans in the range of 1.00–1.65 V vs RHE were performed. Figure 3 shows the electrochemical behavior (in the dark) during the first three CV scans. Although cross-contamination of Pt from the counter electrode is not usually expected to be a problem for OER studies, XPS survey spectra were recorded to rule this out; indeed, no traces of Pt were found on the MnO_x films after electrochemistry (Figure S5). We define a film as OER-active if there is a clear exponential increase in current. Based on this criterion, the 0.7 and 1 nm thick films are not OER-

https://dx.doi.org/10.1021/acsami.0c15977
ACS Appl. Mater. Interfaces 2021, 13, 2428–2436

active. Apparently, those films are too thin to form a catalytically active phase. The minimum MnO_x film thickness for OER activity is 1.5 nm. However, the 1.5 and 2 nm films are not stable; there is no OER current during the second (and third) CV scan. It should be noted that the films do not dissolve; the XPS data for a 1.4 nm film recorded after the electrochemical experiments still shows a very clear Mn signal (Figure S6). Therefore, the films seem to deactivate, the mechanism of which is currently not well understood. The thicker films (4, 6, 7.5, and 10 nm) show OER activity during all three scans, with the highest activity obtained for the 4 and 6 nm thick films.

Investigating the Surface Oxidation. There are no significant differences between the second and third scans, which indicates that these ultrathin films are at least partially conditioned after the second scan. Although the films do not dissolve (Figure S6), it is unclear how fragile they are in this thickness range, so we deliberately avoided extensive cycling. Figure 4a shows the current density for the conditioned anodes

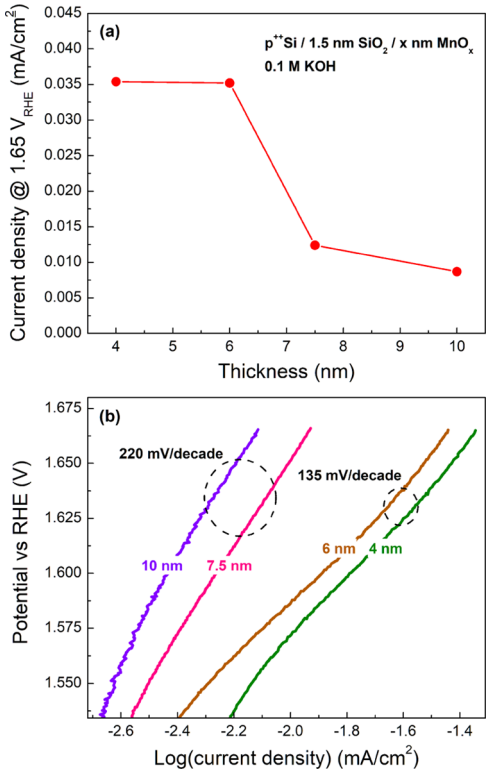

Figure 4. (a) Current density vs film thickness (extracted from the third scan, Figure 3c, at a potential of 1.65 V vs RHE). (b) Tafel slope analysis based on the cyclovoltammogram of Figure 3c.

at a potential of 1.65 V vs RHE, obtained from the third CV scan (Figure 3c). The 4 and 6 nm thick MnO_x anodes show a similar performance. The use of thicker MnO_x films results in a lower current density. This decrease in performance is reflected in the increase in the Tafel slopes (Figure 4b). The Tafel slopes are 135 and 220 mV/dec for the 4–6 and 7.5–10 nm MnO_x anodes, respectively. These values are higher than previously reported slopes for electrodeposited (60 mV/dec)[5,14] and annealed ALD MnO_x films (100 mV/dec).[22] The properties that can affect the electrochemical performance and can also be thickness-dependent include the initial oxidation state of the manganese in the films and the electronic conductivity of the films. The oxidation state of MnO_x is the same for all film thicknesses (see Figure S7); hence, this cannot explain the difference in performance. Strandwitz et al.[32] have seen a decrease in performance for films thicker than 4 nm. They attributed this decrease in performance to an increase in film resistance. In line with Strandwitz et al.,[32] we also attribute the decrease in performance to increasing resistance with increasing film thickness. Note that shunting pathways to the back contact, which were found to play a role in photoactive nanostructured MnO_x-catalyzed $BiVO_4$ films deposited on FTO glass,[38] are unlikely to occur in these smooth and purely electrocatalytic films.

To understand why at least 1.5 nm of MnO_x is needed for OER activity, we studied the behavior of the films just before the onset of water oxidation. Figure 5a shows the cyclo-

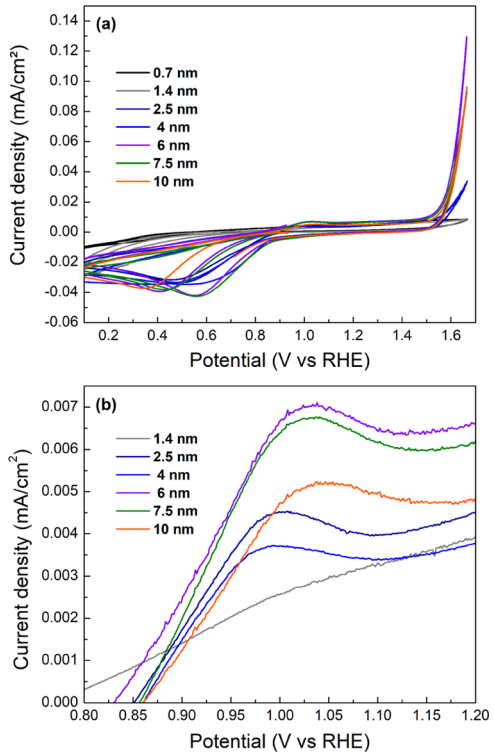

Figure 5. (a) Cyclovoltammograms of Si/MnO_x anodes with different MnO_x thicknesses. (b) Zoom view of the oxidation wave of the MnO_x catalyst film.

voltammograms of p^{++}-Si/MnO_x anodes with different MnO_x film thicknesses in a potential range of 0.10–1.65 V vs RHE. To ensure that the electronic conditions at the surface are the same for each anode, we first scanned in the reverse direction, from the open-circuit potential (OCP, ~0.9 V vs RHE) to a potential of 0.1 V vs RHE. During this reverse sweep, a reduction peak around 0.55 V vs RHE can be observed, which is too large to account for the reduction of the MnO_x film. It is known that MnO_x is capable of reducing oxygen in this potential region.[31] From a CV scan in a nitrogen-purged electrolyte, in which the oxygen reduction peak is suppressed (see Figure S8), we conclude that this reduction peak indeed originates from oxygen reduction. Note that the small amount of dissolved oxygen that might remain after the reverse scan is unlikely to significantly affect the forward scan. After reaching 0.1 V vs RHE, the potential is swept to 1.65 eV vs RHE to see the OER, and then back to the initial OCP. While scanning

https://dx.doi.org/10.1021/acsami.0c15977
ACS Appl. Mater. Interfaces 2021, 13, 2428–2436

from 0.1 V vs RHE toward the OER regime (1.65 V vs RHE), the system crosses a potential where oxidation of the MnO_x catalyst from Mn(II) to Mn(III) is known to occur.[39] We indeed observe this oxidation for 2.5−10 nm thick MnO_x films (Figure 5b). However, even at higher scan rates (up to 50 mV/s), we could not see a distinct oxidation peak for the 0.7 nm (not shown) and 1.4 nm MnO_x films. Both these film thicknesses are below the minimum value needed for OER activity (1.5 nm, *vide supra*). This shows that the OER activity depends on the ability to electrochemically oxidize at least part of the film to the Mn(III) state.

Since all films have the same initial +2 oxidation state after exposure to air (Figure S7), the absence of the Mn(II) → Mn(III) oxidation peak for the 0.7 and 1.4 nm films is surprising. We tentatively attribute this behavior to a different electron density distribution at the Si/MnO_x interface compared to bulk MnO_x. Due to the higher electronegativity of Si (1.90 on the Pauling scale) compared to Mn (1.55), the electron density around the Mn atoms is expected to decrease when approaching the Si/MnO_x interface. This decrease in electron density would increase the binding energy of Mn core electrons, making it more difficult to oxidize MnO_x thin films. We indeed observe a shift of the Mn $2p_{3/2}$ peak toward higher binding energies for decreasing MnO_x film thickness, as shown in Figure 6a,b. The shift in binding energy only occurs in the ultrathin-film range (<2 nm), while thicker films are not affected. Note that this increase in binding energy cannot be simply explained by a higher oxidation state of the thinnest films. This is because the shift in BE in Figure 6 occurs for as-deposited films under UHV conditions, whereas all films exposed to air show the +2 oxidation state (Figure S7); it is extremely unlikely that exposure to air would result in a reduction of Mn from +3 or +4 to +2. These observations provide compelling support for our explanation that ultrathin (<2 nm) MnO_x films show lower OER activity due to the electrostatic influence of the substrate.

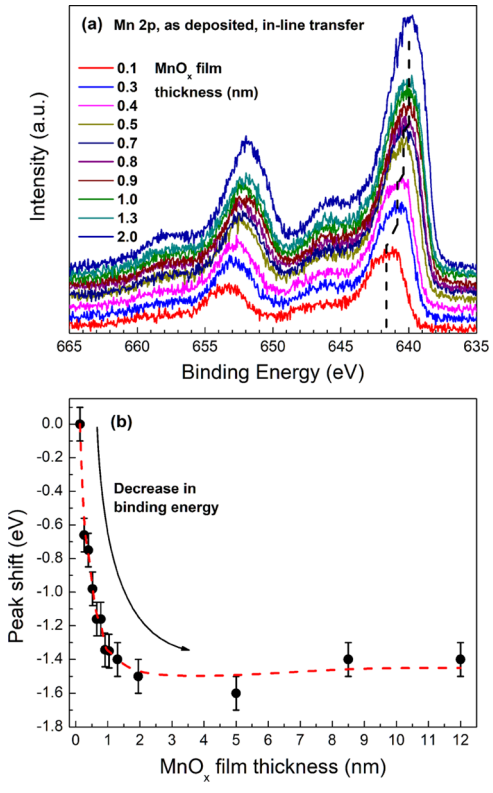

Figure 6. (a) Mn 2p fine spectra of ultrathin (<2 nm) MnO_x films. (b) Peak shift of the Mn $2p_{3/2}$ peak relative to the peak position of the 0.1 nm MnO_x film.

We also briefly consider an alternative explanation, which is that the thinnest films are somehow unable to undergo the required structural transformations during (or just before the onset of) the oxygen evolution reaction. Although the films are known to be hydroxylated (*vide supra*), we cannot rule out this possibility. Theoretical calculations may help to answer this question, but are beyond the scope of this study. It seems unlikely, however, that any difficulties in structural transformations can explain the observed absence of a more simple redox-type oxidation of Mn. Based on the observed shift in binding energy in Figure 6a, our explanation in terms of electrostatic interaction with the substrate seems more likely.

The area under the manganese oxidation peak (Figure 5) is equal to the amount of charge transferred from the manganese oxide film to the back contact and is, therefore, proportional to the number of oxidized manganese atoms. The peak area was found to saturate for films thicker than 2.5 nm (see Figure S9c). This implies that the same amount of MnO_x is oxidized during the potential sweep, regardless of film thickness. Because our ALD films are compact and well defined, the number of oxidized manganese atoms can be converted into a film thickness. Following the conclusion drawn from XPS (Figure 2c), the oxidation peak represents the transformation of Mn(II) to a mix of Mn(III) and Mn(IV). For the sake of simplicity, it is assumed that the average oxidation state after electrochemistry is equal to +3.5. This means that on average, 1.5 electrons per manganese atom are transferred. With this information and the area of the oxidation peak, we can calculate the amount of oxidized Mn atoms and, therefore, a thickness of the oxidized film (d_{ox}). The assumptions and equations for this calculation can be found in the Supporting Information.

Figure 7 shows the calculated thickness of the electrochemically oxidized films, which saturates at 0.19 ± 0.02 nm for films thicker than 2.0 nm. This corresponds to one monolayer of MnO as the Mn−O distances in MnO_x vary between 0.18 and 0.23 nm. In Mn(II)O, this value is close to the Mn−O distance of 0.225 nm. This leads to the conclusion that one monolayer of oxidizable manganese atoms is sufficient to get OER activity. This is indeed in line with previous reports.[4,40] However, since

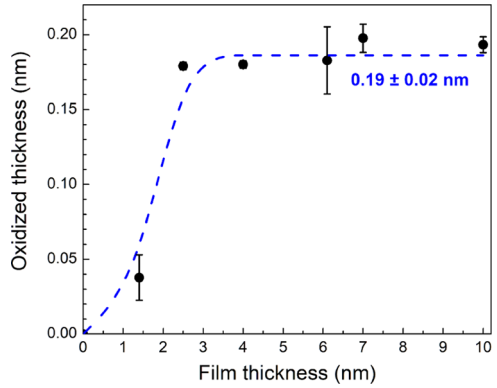

Figure 7. Calculated oxidized thickness vs film thickness. The dashed blue line serves as a guide to the eye.

https://dx.doi.org/10.1021/acsami.0c15977
ACS Appl. Mater. Interfaces 2021, 13, 2428−2436

the aforementioned influence of the silicon substrate prevents oxidation of manganese atoms near the Si/MnO_x interface, a film thickness of at least 1.5−2 nm is needed to escape the influence of the underlying substrate and enable oxidation of the film. This explains why films thinner than the 1.5−2 nm threshold show no OER activity.

The insight that a certain amount of oxidizable Mn ions needs to be present explains why films thinner than 1.5 nm are not OER-active. It does not explain, however, *why* oxidation of MnO_x leads to better performance. To investigate this, we studied the valence band structure of partially oxidized MnO_x films with UPS. Since UPS is more surface sensitive than XPS, a clean surface is needed to make sure that the valence band signal is not dominated by surface contaminations. As a consequence, films already used for electrochemistry cannot be examined, as the surface will always contain electrolyte residue. Any attempts to remove this residue by heat treatment or Ar sputtering would change the band structure of the MnO_x film. Therefore, we mimic the electrochemical oxidation process in our in-line ALD/XPS reactor by exposing a 12 nm MnO_x film to an O_2 plasma. Figure 8a shows Mn 2p fine spectra of the plasma-treated MnO_x film. The Mn 2p spectrum of the plasma-exposed film was best fitted with the MnO_2 multiplet pattern,[37] accompanied by an additional peak at 640.5 eV binding energy. The 11 eV separation between the Mn $2p_{1/2}$ peak and its satellite indeed confirms that the +IV oxidation state is the dominant one.[23] The spectrum is nearly identical to that of the MnO_x sample after electrochemical oxidation (Figure 2c). It should be noted, however, that the plasma-treated samples may no longer be −OH-terminated, so the actual surfaces of the plasma- and electrochemically treated samples may be different, despite the almost identical Mn 2p spectra.

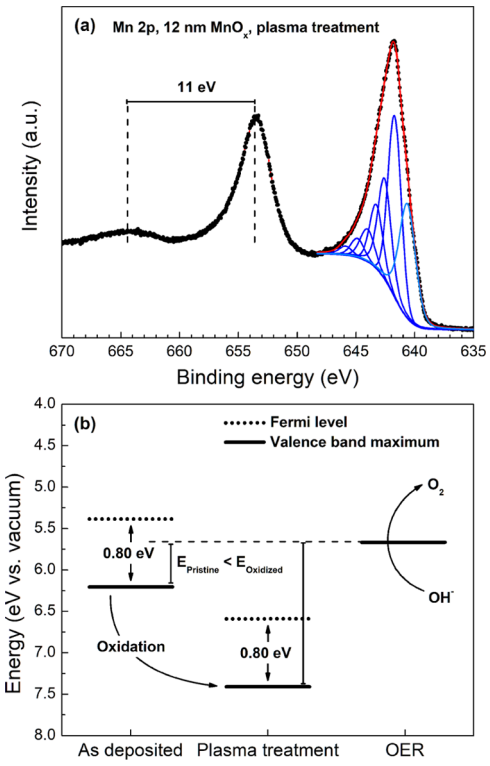

Figure 8. (a) Mn 2p fine spectra of plasma-exposed MnO_x film. (b) Fermi level and VBM with respect to the vacuum level for as-deposited and plasma-exposed films. The preparation details can be found in the Supporting Information.

The valence band maxima of the as-deposited film (MnO_x, with Mn mainly in the +II state) and the plasma-treated film (MnO_2) are compared in Figure S10a. Extrapolation of the valence band edges yields similar values (~0.8 eV below the Fermi level), although the plasma-treated sample shows a tail of occupied states all the way up to the Fermi level. A much bigger difference, however, is observed for the work function, which is ~1.2 eV larger for the plasma-exposed film than for the as-deposited film (see Figure S10b). This is due to either oxidation of the manganese ions, which shifts the energy levels of the manganese oxide film to lower values, but it might also be affected by differences in the degree of surface hydroxylation. Either way, the higher work function corresponds to an anodic shift with respect to the OER level, which increases the thermodynamic driving force for water oxidation (Figure 8b). This offers a possible explanation why the oxidation of MnO_x is necessary to form an active catalyst.

CONCLUSIONS

We have studied the origin of the OER activity of ultrathin MnO_x films under alkaline conditions. A minimum MnO_x thickness of 1.5 nm is found to be necessary to get OER-active films, while a thickness >2 nm is needed for the films to be stable beyond the first cyclic voltammogram. The highest OER current is obtained with 4−6 nm MnO_x films. The OER current decreases for thicker films, which we attribute to an increase in film resistance. XPS analysis shows that the oxidation state of the manganese ions changes from +II to +III/+IV prior to the OER. We found that the number of Mn(II) ions oxidized corresponds to 0.19 nm MnO_x (~1 monolayer), which is in agreement with previous reports.[4,40] This suggests that a monolayer of MnO_x should already be OER-active. However, the high electronegativity of the silicon atoms in the substrate affects neighboring Mn ions and increases their binding energy. As a result, the manganese ions within an ~1 nm distance from the Si/MnO_x interface are more difficult to oxidize than Mn ions further away from this interface. This explains why films thinner than 1.5 nm are not OER-active. To avoid this limitation, the electronegativity of the support should be less than that of the OER catalyst to allow facile oxidation of the manganese ions close to the catalyst/support interface. These insights illustrate the importance of catalyst/support interactions in electrocatalysis and provide useful design guidelines for ultrathin MnO_x-based OER catalysts.

ASSOCIATED CONTENT

Supporting Information

The Supporting Information is available free of charge at https://pubs.acs.org/doi/10.1021/acsami.0c15977.

Growth per cycle curves for ALD-deposited MnO_x films under various process conditions; original TEM data; AFM images; additional XPS and UPS spectra; tables with XPS fitting parameters; CV scan with a N_2-purged electrolyte; and detailed information on the calculation of the amount of oxidized Mn atoms and the corresponding oxidized film thickness (PDF)

https://dx.doi.org/10.1021/acsami.0c15977
ACS Appl. Mater. Interfaces 2021, 13, 2428−2436

AUTHOR INFORMATION

Corresponding Author

Roel van de Krol − *Institute for Solar Fuels, Helmholtz-Zentrum Berlin für Materialien und Energie GmbH, 14109 Berlin, Germany; Institut für Chemie, Technische Universität Berlin, 10623 Berlin, Germany;* orcid.org/0000-0003-4399-399X; Email: roel.vandekrol@helmholtz-berlin.de

Authors

Paul Plate − *Institute for Solar Fuels, Helmholtz-Zentrum Berlin für Materialien und Energie GmbH, 14109 Berlin, Germany*

Christian Höhn − *Institute for Solar Fuels, Helmholtz-Zentrum Berlin für Materialien und Energie GmbH, 14109 Berlin, Germany*

Ulrike Bloeck − *Institute for Solar Fuels, Helmholtz-Zentrum Berlin für Materialien und Energie GmbH, 14109 Berlin, Germany*

Peter Bogdanoff − *Institute for Solar Fuels, Helmholtz-Zentrum Berlin für Materialien und Energie GmbH, 14109 Berlin, Germany*

Sebastian Fiechter − *Institute for Solar Fuels, Helmholtz-Zentrum Berlin für Materialien und Energie GmbH, 14109 Berlin, Germany*

Fatwa F. Abdi − *Institute for Solar Fuels, Helmholtz-Zentrum Berlin für Materialien und Energie GmbH, 14109 Berlin, Germany;* orcid.org/0000-0001-5631-0620

Aafke C. Bronneberg − *Institute for Solar Fuels, Helmholtz-Zentrum Berlin für Materialien und Energie GmbH, 14109 Berlin, Germany*

Complete contact information is available at: https://pubs.acs.org/10.1021/acsami.0c15977

Author Contributions

The manuscript was written through contributions of all authors. All authors have given approval to the final version of the manuscript.

Funding

This work was supported by the German Bundesministerium für Bildung and Forschung (BMBF), project "MANGAN" (03SF0505).

Notes

The authors declare no competing financial interest.

ACKNOWLEDGMENTS

The authors acknowledge Dr. Marco Favaro for his assistance with the interpretation of valence band spectra.

ABBREVIATIONS USED

ALD, atomic layer deposition
PEC, photoelectrochemistry
UPS, ultraviolet photoelectron spectroscopy
XPS, X-ray photoelectron spectroscopy
CV, cyclovoltammometry
OER, oxygen evolution reaction
VBM, valence band maximum
RHE, reversible hydrogen electrode
OER, oxygen evolution reaction
OCP, open-circuit potential
TEM, transmission electron microscopy
EtCp, ethyl-cyclopentadienyl
GPC, growth per cycle
SE, spectroscopic ellipsommetry

REFERENCES

(1) van de Krol, R.; Parkinson, B. A. Perspectives on the Photoelectrochemical Storage of Solar Energy. *MRS Energy Sustainability* **2017**, *4*, No. E13.

(2) Reece, S. Y.; Hamel, J. A.; Sung, K.; Jarvi, T. D.; Esswein, A. J.; Pijpers, J. J. H.; Nocera, D. G. Wireless Solar Water Splitting Using Silicon-Based Semiconductors and Earth-Abundant Catalysts. *Science* **2011**, *334*, 645−648.

(3) Maeda, K.; Xiong, A. K.; Yoshinaga, T.; Ikeda, T.; Sakamoto, N.; Hisatomi, T.; Takashima, M.; Lu, D. L.; Kanehara, M.; Setoyama, T.; Teranishi, T.; Domen, K. Photocatalytic Overall Water Splitting Promoted by Two Different Cocatalysts for Hydrogen and Oxygen Evolution under Visible Light. *Angew. Chem., Int. Ed.* **2010**, *49*, 4096−4099.

(4) Ramírez, A.; Hillebrand, P.; Stellmach, D.; May, M. M.; Bogdanoff, P.; Fiechter, S. Evaluation of MnO_x, Mn_2O_3, and Mn_3O_4 Electrodeposited Films for the Oxygen Evolution Reaction of Water. *J. Phys. Chem. C* **2014**, *118*, 14073−14081.

(5) Kölbach, M.; Fiechter, S.; van de Krol, R.; Bogdanoff, P. Evaluation of Electrodeposited α-Mn_2O_3 as a Catalyst for the Oxygen Evolution Reaction. *Catal. Today* **2017**, *290*, 2−9.

(6) Dau, H.; Grundmeier, A.; Loja, P.; Haumann, M. On the Structure of the Manganese Complex of Photosystem II: Extended-Range EXAFS Data and Specific Atomic-Resolution Models for Four S-States. *Philos. Trans. R. Soc., B* **2008**, *363*, 1237−1243.

(7) Wiechen, M.; Berends, H. M.; Kurz, P. Water Oxidation Catalysed by Manganese Compounds: from Complexes to 'Biomimetic Rocks'. *Dalton Trans.* **2012**, *41*, 21−31.

(8) Morita, M.; Iwakura, C.; Tamura, H. The Anodic Characteristics of Manganese Dioxide Electrodes Prepared by Thermal Decomposition of Manganese Nitrate. *Electrochim. Acta* **1977**, *22*, 325−328.

(9) Frey, C. E.; Wiechen, M.; Kurz, P. Water-Oxidation Catalysis by Synthetic Manganese Oxides - Systematic Variations of the Calcium Birnessite Theme. *Dalton Trans.* **2014**, *43*, 4370−4379.

(10) Huynh, M.; Shi, C. Y.; Billinge, S. J. L.; Nocera, D. G. Nature of Activated Manganese Oxide for Oxygen Evolution. *J. Am. Chem. Soc.* **2015**, *137*, 14887−14904.

(11) Huynh, M.; Bediako, D. K.; Nocera, D. G. A Functionally Stable Manganese Oxide Oxygen Evolution Catalyst in Acid. *J. Am. Chem. Soc.* **2014**, *136*, 6002−6010.

(12) Ramírez, A.; Friedrich, D.; Kunst, M.; Fiechter, S. Charge Carrier Kinetics in MnO_x, Mn_2O_3 and Mn_3O_4 Films for Water Oxidation. *Chem. Phys. Lett.* **2013**, *568*, 157−160.

(13) Takashima, T.; Hashimoto, K.; Nakamura, R. Mechanisms of pH-Dependent Activity for Water Oxidation to Molecular Oxygen by MnO_2 Electrocatalyst. *J. Am. Chem. Soc.* **2012**, *134*, 1519−1527.

(14) Zaharieva, I.; Chernev, P.; Risch, M.; Klingan, K.; Kohlhoff, M.; Fischer, A.; Dau, H. Electrosynthesis, Functional, and Structural Characterization of a Water-Oxidizing Manganese Oxide. *Energy Environ. Sci.* **2012**, *5*, 7081−7089.

(15) Kumbhar, V. S.; Lee, H.; Lee, J.; Lee, K. Recent Advances in Water-Splitting Electrocatalysts Based on Manganese Oxide. *Carbon Resour. Convers.* **2019**, *2*, 242−255.

(16) Melder, J.; Bogdanoff, P.; Zaharieva, I.; Fiechter, S.; Dau, H.; Kurz, P. Water-Oxidation Electrocatalysis by Manganese Oxides: Syntheses, Electrode Preparations, Electrolytes and Two Fundamental Questions. *Z. Phys. Chem.* **2020**, *234*, 925−978.

(17) van Oversteeg, C. H. M.; Doan, H. Q.; de Groot, F. M. F.; Cuk, T. In Situ X-ray Absorption Spectroscopy of Transition Metal Based Water Oxidation Catalysts. *Chem. Soc. Rev.* **2017**, *46*, 102−125.

(18) Gorlin, Y.; Lassalle-Kaiser, B.; Benck, J. D.; Gul, S.; Webb, S. M.; Yachandra, V. K.; Yano, J.; Jaramillo, T. F. In Situ X-ray Absorption Spectroscopy Investigation of a Bifunctional Manganese Oxide Catalyst with High Activity for Electrochemical Water Oxidation and Oxygen Reduction. *J. Am. Chem. Soc.* **2013**, *135*, 8525−8534.

(19) Wiechen, M.; Zaharieva, I.; Dau, H.; Kurz, P. Layered Manganese Oxides for Water-Oxidation: Alkaline Earth Cations Influence Catalytic Activity in a Photosystem II-Like Fashion. *Chem. Sci.* **2012**, *3*, 2330−2339.
(20) Ramírez, A.; Bogdanoff, P.; Friedrich, D.; Fiechter, S. Synthesis of $Ca_2Mn_3O_8$ Films and Their Electrochemical Studies for the Oxygen Evolution Reaction (OER) of Water. *Nano Energy* **2012**, *1*, 282−289.
(21) Najafpour, M. M.; Ehrenberg, T.; Wiechen, M.; Kurz, P. Calcium Manganese(III) Oxides ($CaMn_2O_4.xH_2O$) as Biomimetic Oxygen-Evolving Catalysts. *Angew. Chem., Int. Ed.* **2010**, *49*, 2233−2237.
(22) Mattelaer, F.; Bosserez, T.; Ronge, J.; Martens, J. A.; Dendooven, J.; Detavernier, C. Manganese Oxide Films with Controlled Oxidation State for Water Splitting Devices Through a Combination of Atomic Layer Deposition and Post-Deposition Annealing. *RSC Adv.* **2016**, *6*, 98337−98343.
(23) Gorlin, Y.; Jaramillo, T. F. A Bifunctional Nonprecious Metal Catalyst for Oxygen Reduction and Water Oxidation. *J. Am. Chem. Soc.* **2010**, *132*, 13612−13614.
(24) Julien, C.; Massot, M.; Baddour-Hadjean, R.; Franger, S.; Bach, S.; Pereira-Ramos, J. P. Raman Spectra of Birnessite Manganese Dioxides. *Solid State Ionics* **2003**, *159*, 345−356.
(25) Li, A. L.; Ooka, H.; Bonnet, N.; Hayashi, T.; Sun, Y. M.; Jiang, Q. K.; Li, C.; Han, H. X.; Nakamura, R. Stable Potential Windows for Long-Term Electrocatalysis by Manganese Oxides Under Acidic Conditions. *Angew. Chem., Int. Ed.* **2019**, *58*, 5054−5058.
(26) Rabe, M.; Toparli, C.; Chen, Y. H.; Kasian, O.; Mayrhofer, K. J. J.; Erbe, A. Alkaline Manganese Electrochemistry Studied by In Situ and Operando Spectroscopic Methods - Metal Dissolution, Oxide Formation and Oxygen Evolution. *Phys. Chem. Chem. Phys* **2019**, *21*, 10457−10469.
(27) Tesch, M. F.; Bonke, S. A.; Jones, T. E.; Shaker, M. N.; Xiao, J.; Skorupska, K.; Mom, R.; Melder, J.; Kurz, P.; Knop-Gericke, A.; Schlogl, R.; Hocking, R. K.; Simonov, A. N. Evolution of Oxygen-Metal Electron Transfer and Metal Electronic States During Manganese Oxide Catalyzed Water Oxidation Revealed with In Situ Soft X-Ray Spectroscopy. *Angew. Chem., Int. Ed.* **2019**, *58*, 3426−3432.
(28) Shaker, M. N.; Bonke, S. A.; Xiao, J.; Khan, M. A.; Hocking, R. K.; Tesch, M. F. Insight into pH-Dependent Formation of Manganese Oxide Phases in Electrodeposited Catalytic Films Probed by Soft X-Ray Absorption Spectroscopy. *ChemPlusChem* **2018**, *83*, 721−727.
(29) Frey, C. E.; Kwok, F.; Gonzales-Flores, D.; Ohms, J.; Cooley, K. A.; Dau, H.; Zaharieva, I.; Walter, T. N.; Simchi, H.; Mohney, S. E.; Kurz, P. Evaporated Manganese Films as a Starting Point for the Preparation of Thin-Layer MnO_x Water-Oxidation Anodes. *Sustainable Energy Fuels* **2017**, *1*, 1162−1170.
(30) Burton, B. B.; Fabreguette, F. H.; George, S. M. Atomic Layer Deposition of MnO Using Bis(ethylcyclopentadienyl) Manganese and H_2O. *Thin Solid Films* **2009**, *517*, 5658−5665.
(31) Pickrahn, K. L.; Park, S. W.; Gorlin, Y.; Lee, H. B. R.; Jaramillo, T. F.; Bent, S. F. Active MnO_x Electrocatalysts Prepared by Atomic Layer Deposition for Oxygen Evolution and Oxygen Reduction Reactions. *Adv. Energy Mater.* **2012**, *2*, 1269−1277.
(32) Strandwitz, N. C.; Comstock, D. J.; Grimm, R. L.; Nichols-Nielander, A. C.; Elam, J.; Lewis, N. S. Photoelectrochemical Behavior of n-type Si(100) Electrodes Coated with Thin Films of Manganese Oxide Grown by Atomic Layer Deposition. *J. Phys. Chem. C* **2013**, *117*, 4931−4936.
(33) Du, L. Y.; Yu, S. S.; Liu, X. F.; Ding, Y. Q. An Efficient Atomic Layer Deposition Process of MnO_x Films Using Bis(N,N'-di-tert-Butylacetamidinato)Manganese-(II) and H_2O as Reactants. *Appl. Surf. Sci.* **2019**, *486*, 460−465.
(34) Bronneberg, A. C.; Hohn, C.; van de Krol, R. Probing the Interfacial Chemistry of Ultrathin ALD-Grown TiO_2 Films: An In-Line XPS Study. *J. Phys. Chem. C* **2017**, *121*, 5531−5538.
(35) Langereis, E.; Heil, S. B. S.; Knoops, H. C. M.; Keuning, W.; van de Sanden, M. C. M.; Kessels, W. M. M. In Situ Spectroscopic Ellipsometry as a Versatile Tool for Studying Atomic Layer Deposition. *J. Phys. D: Appl. Phys.* **2009**, *42*, No. 073001.
(36) Holleman, A. F.; Wiberg, E.; Wiberg, N. *Lehrbuch der Anorganischen Chemie*, 102nd ed.; de Gruyter: Berlin, 2007.
(37) Biesinger, M. C.; Payne, B. P.; Grosvenor, A. P.; Lau, L. W. M.; Gerson, A. R.; Smart, R. S. Resolving Surface Chemical States in XPS Analysis of First Row Transition Metals, Oxides and Hydroxides: Cr, Mn, Fe, Co and Ni. *Appl. Surf. Sci.* **2011**, *257*, 2717−2730.
(38) Irani, R.; Plate, P.; Hohn, C.; Bogdanoff, P.; Wollgarten, M.; Höflich, K.; van de Krol, R.; Abdi, F. F. The Role of Ultra-Thin MnO_x Co-Catalysts on the Photoelectrochemical Properties of $BiVO_4$ Photoanodes. *J. Mater. Chem. A* **2020**, *8*, 5508−5516.
(39) Lima, F. H. B.; Calegaro, M. L.; Ticianelli, E. A. Electrocatalytic Activity of Manganese Oxides Prepared by Thermal Decomposition for Oxygen Reduction. *Electrochim. Acta* **2007**, *52*, 3732−3738.
(40) Hillebrand, P.; Ramirez-Caro, A.; Calvet, W.; Bogdanoff, P.; Fiechter, S. On the Structure-Function Relationship of Cobalt and Manganese Oxides as Oxygen Evolving Catalysts for Light-Driven Water Electrolysis: An In-Line Synchrotron Radiation Photoelectron Spectroscopy Study. *ECS Trans.* **2014**, *61*, 9−20.

https://dx.doi.org/10.1021/acsami.0c15977
ACS Appl. Mater. Interfaces 2021, 13, 2428−2436